Towards high-resolution measurements of turbulent compressible shear layers using a novel nano-scale sensor

By S. Duvvuri†, K. Kokmanian†, M. Hultmark†, S. Scharnowski‡, M. Bross‡ AND C.J. Kähler‡

† Mechanical & Aerospace Engineering Department, Princeton University
Princeton, New Jersey 08544, USA

‡ Institute for Fluid Mechanics and Aerodynamics, Universität der Bundeswehr München
Neubiberg 85579, Germany

This report outlines a measurement campaign carried out at the Trisonic Wind Tunnel Munich (TWM) facility with novel nano-scale thermal anemometry sensors that were employed for the first time in compressible flow conditions, in the Mach number (M) range $0.3 < M < 2$. This effort combines the expertise of Princeton University in design, fabrication, and application of nano-scale flow sensors with the unique experimental facilities at Bundeswehr University. The results demonstrate the utility of the sensors in providing turbulence spectral information and the scope for further design improvements. Overall, the outcome from this campaign shows great promise towards the development of robust high-resolution point-measurement capabilities that neatly complement existing particle image velocimetry (PIV) techniques in compressible flows.

1. Introduction

The dynamics of velocity fluctuations in incompressible shear turbulence are immensely complex given the highly multi-scale and non-linear nature of the problem. In the compressible flow regime, like in supersonic boundary layer or wake flows, the problem is further compounded by turbulent fluctuations in temperature and density fields in addition to velocity fluctuations, and their coupling. Thus, it is perhaps not surprising that relatively limited progress has been made in studies of compressible shear flows in comparison with their incompressible counterparts [1]. Given the numerous relevant aerospace engineering applications, particularly with regard to space transportation systems, there is a clear motivation to make research progress at a fundamental level in the area of compressible shear turbulence.

Well-refined experimental data is a key requirement for advancing our theoretical understanding in such flow configurations, and also in aiding model development for computational studies and their subsequent validation. The challenging flow environment and short time scales encountered at supersonic conditions typically restrict the ability to acquire experimental data that fully resolves the physical quantities of interest. In recent times, PIV has been employed as the main tool in experimental investigations of high-speed flows; PIV can provide instantaneous flow fields (velocity vectors over a set spatial domain) and also turbulence statistics in a measurement plane or volume [2, 3]. However, current PIV techniques are limited in their spatial and temporal resolution and lack the ability to resolve the full turbulence spectrum. Hence, point measurements that are fully resolved in the temporal domain would greatly complement PIV.

With this motivation, we attempt to use a novel nano-scale thermal anemometry sensor for measurements in compressible flows. The probe design builds on previous development efforts at Princeton University in the area of nano-scale measurement devices for incompressible flows [4–6]. The sensors were fabricated in-house using well-established semiconductor and MEMS manufacturing methods. They operate on the same physical principle as a conventional hot-/cold-wire – the flow condition is informed by changes in voltage or electrical resistance of a small current-carrying wire element that is exposed to the flow. Relative to a conventional hot-/cold-wire, the reduced size and thermal inertia of a nano-scale sensor greatly improves its spatio-temporal resolution, which makes it particularly well-suited for application in a supersonic flow setting. These features have previously been exploited to obtain fully-resolved velocity spectral data in incompressible wall turbulence at high Reynolds numbers (see [7] for instance). For the first time, we adapt the probe design for measurements in high-subsonic and supersonic conditions. Details of the experimental setup and sensors are provided in section 2. Measurements were made to characterize the free-stream turbulence levels in subsonic conditions at Mach numbers $M = 0.3, 0.5, 0.8$, and to characterize the heat transfer behavior of the sensor in supersonic conditions up to $M = 2$. Preliminary boundary layer measurements on a flat plate model along with velocity and wall-pressure correlations were also made at $M = 0.8$. Results from these experiments are presented in section 3, followed by brief concluding remarks in section 4.

2. Experimental Facility and Measurement Methods

2.1. *Trisonic Wind Tunnel Munich (TWM)*

The TWM is a blow-down wind tunnel with a test section that is 1700 mm long with a cross-section of 300 mm $\times$ 675 mm (width $\times$ height). The test section is enclosed by a plenum chamber with the ability to apply boundary layer suction at both the vertical and horizontal walls independently. A two-throat system consisting of an adjustable-geometry de Laval nozzle upstream and an adjustable-geometry diffuser downstream of the test section allows for stable operating Mach numbers in the range $0.15 < M < 3.0$. The stagnation pressure p_0 is controlled by a regulator valve and can be set between $p_0 = 1.2$ bar and 5.0 bar. This set up allows for the test section Reynolds number (mass flow rate) to be set independently of the Mach number; the corresponding Reynolds number range is $(4 - 80) \times 10^7$ m^{-1}. Note that both the Reynolds number and the Mach number can be varied during the course of tunnel operation by actively changing the stagnation pressure and the nozzle/diffuser geometry. This is an important aspect of the facility as it allows for a smooth start-up and shutdown of test section flow in terms of the structural loading on the sensors. For supersonic conditions, the start-up shock wave can be made to pass through the test section at a very low supersonic Mach number (close to 1) to minimize the shock strength, before ramping up the Mach number to the desired value ($M = 2$ in the present experiments). The tunnel stagnation chamber is supplied by two storage tanks that can be pressurized up to 20 bar above ambient pressure, with each tank holding a volume of 178 m^3 of air. The air mass in the tanks at full pressure allows for run times on the order of 100 seconds for the flow conditions used in these experiments. Figure 1 gives an overview of the wind tunnel. See [8] for further details on this facility. The flat plate model used in the present experiments is described in the following sub-section.

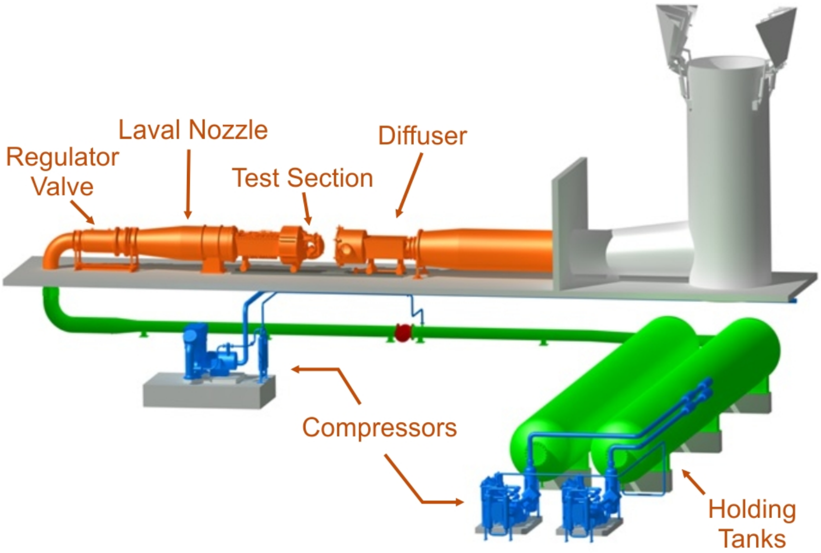

FIGURE 1. A schematic of the Trisonic Wind Tunnel Munich. Some of the facility features discussed in the text are identified here.

2.2. *Flat Plate Model*

The aerodynamic performance of many aerospace vehicles is directly dependent on the behavior of the airframe turbulent boundary layers. For this reason, the physical understanding of wall-bounded shear flows is of great scientific interest and technological importance. Therefore, a flat plate boundary layer model was used as the test model for this investigation. The aluminum flat plate, shown in figure 2, was designed to span the entire allowable length of the test section to maximize the development length and yield the thickest possible boundary layer close to the trailing edge. In this case, the flat plate has dimensions of 1700 mm and 300 mm in the streamwise and spanwise directions respectively. The leading edge of the plate is sharp so that an attached shock occurs right at the leading edge during supersonic conditions, and that minimizes any undesired shock boundary layer interactions. Preliminary Schlieren and PIV measurements estimate the boundary layer thickness to be around 12 mm at a streamwise location of 1300 m downstream of the leading edge. This value of the layer thickness remains relatively constant for the range of Mach and Reynolds numbers investigated herein. In order to measure the static pressures along the plate, several equidistantly spaced pressure ports were installed from the leading edge to the trailing edge of the model along the mid-span (centerline). Furthermore, to record the unsteady pressure signal at the wall in a time-resolved manner, dynamic pressure sensors (Kulite XCQ-062) with a frequency response of 25 kHz were also installed in a T-shaped pattern approximately 1300 mm downstream of the leading edge, as illustrated in figure 2.

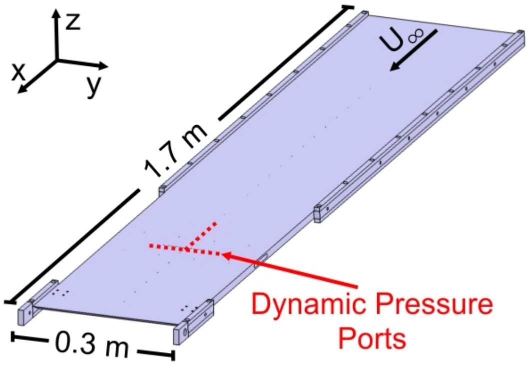

FIGURE 2. A schematic of the flat plate boundary layer model. The axis along the streamwise, spanwise, and wall-normal directions are denoted by x, y, z respectively. U_∞ denotes the free-stream velocity in the streamwise direction.

2.3. *Nano-Scale Thermal Anemometry Probe*

The nano-scale thermal anemometry probe (henceforth referred to as NSTAP) was first developed in 2006 [9]. The objective was to design and manufacture a nano-scale hot-wire which could be used in high Reynolds number test facilities, such as the Princeton Superpipe, to capture spectral information over a wide range of scales in the flow [10]. As the Reynolds number increases in a fixed-size facility, the necessity of using a sensing element (or wire) with the smallest possible length scale arises as the smaller scales of energetic turbulence continue to decrease in physical size. In order to mitigate spatial filtering, the size of the sensing element must be on the order of the smallest 'eddies' present in the flow [6]. Therefore, a micro-electro-mechanical system (MEMS) approach was utilized to construct the NSTAP in the micro-/nano-fabrication laboratory at Princeton University. It is to be noted that the thermal inertia of the sensing element goes down with its physical size, and thereby the temporal frequency response goes up. The high temporal resolution afforded by the nano-scale sensing element is particularly attractive in supersonic flow scenarios, where the time scales of interest are typically very small. The fabrication process and sensor geometry are described below.

2.3.1. *Fabrication Process*

The NSTAP base consists of a silicon substrate with a thin layer of silicon dioxide deposited on top. With the use of photolithography, a two-dimensional design is patterned onto the substrate. A layer of metal is then sputtered onto the latter, the thickness of which can vary depending on the final sensor requirements. Platinum is most often the metal of choice due to its relatively low thermal conductivity. Upon performing a lift-off process, the metal only adheres to the areas without photoresist (see [10] for further details). The next steps involve etching processes in order to release the sensing element from the substrate. Deep reactive ion etching (DRIE) is performed alongside an RIE lag in order to etch through silicon while achieving an attractive aerodynamic shape – see figure 3. Upon etching, the sensing element is released from the silicon base and is solely supported by metallic stubs on either ends. Prior to usage, the silicon dioxide must be removed from the sensor in order for the heating element to be completely free-standing; this is achieved with the use of a buffered oxide etchant (BOE). Finally, the sensor is soldered onto copper-plated prongs and integrated into the test facility. A custom sting was fabricated to mount the prongs in the test section (see figure 4).

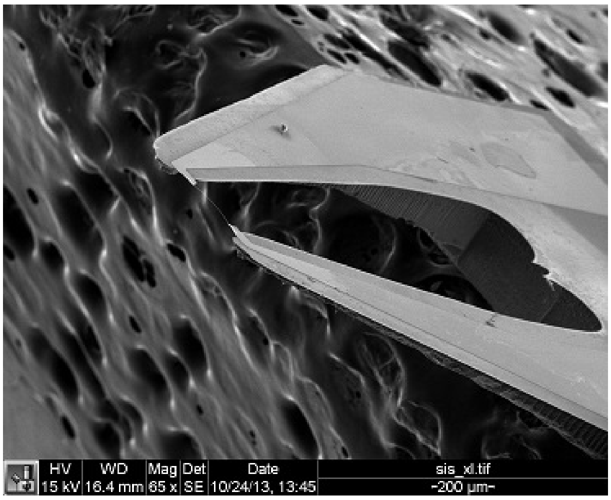

FIGURE 3. A representative scanning electron microscope (SEM) image of a NSTAP. Seen here is the silicon substrate with a thin layer of platinum deposited on top. The active heating element – the thin platinum wire upstream of the silicon base – is supported by platinum stubs on both ends. Electric current is passed through the wire during operation to heat it to a preset temperature.

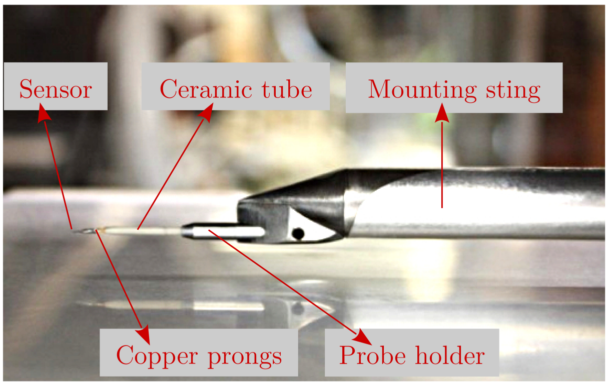

FIGURE 4. A photograph of the test section that shows the sensor integration. The sensor, similar to the one shown in figure 3, is at the front of the assembly (the flow goes from left to right). The sting is mounted to a traverse (not seen in this photograph) which allows for the sensor to be positioned at various streamwise (x) and wall-normal (z) positions along the test section mid-span.

2.3.2. *Sensor Geometric Variants and Operation*

The NSTAPs used in most of the previous studies in incompressible flow conditions had sensing elements that were 200 μm long (in y), 2 μm wide (in x) and 100 nm thick (in z). In supersonic flows however, the structural loading on the wire was estimated to be much higher from simple scaling arguments. To mitigate the risk of sensor breakage during tunnel start-up and operation, the geometry of the sensing element was suitably modified. A few different geometric variants were fabricated and tested during the course of this measurement campaign. Firstly, the active length was reduced to two values – 30 µm and 60 µm. For each of these lengths, sensors were fabricated in two further thicknesses – 100 nm and 500 nm thick platinum – thereby giving a total of four variants. The wire width was kept constant at 2 µm in all cases. Finally, for each of these designs, a portion of the sensors used in the TWM tests were only partially etched. In such sensors, the sensing element is only exposed fully on one side (on the x-y plane), while the other side retains a thin layer of silicon dioxide (500 nm) under a layer of silicon (approximately 10 µm) which provides structural support. The silicon dioxide dampens the frequency response of the sensor to some extent due to heat conduction effects and added thermal inertia. However, owing to the overall small scale of the sensing element, the frequency response was still found to be satisfactory, and limited only by the anemometer circuit and not the sensor.

All of the sensor design variants described above were tested in the present campaign in various flow conditions (varying both Mach and Reynolds numbers). The 30 µm long, 500 nm thick, and partially etched sensors were found to be the most robust in terms of structural integrity and suffered minimal breakages during experimentation. Hence, all the data presented in this report was acquired using this sensor variant.

The sensors were operated in constant temperature (CTA) mode using a Dantec Streamline anemometer (90N10 frame) with a 90C10 CTA module. The overheat ratio, defined here as the ratio of the hot- to cold-wire resistances, was set to a value around 1.2 in all experiments. Square-wave response tests carried out with the sensors exposed to flow in the test section estimated the frequency response to be around 200 kHz. The anemometer voltage output was digitally acquired using a Dewetron DEWE-50-PCI-16 with a DAQP-STG card at a sampling rate of 100 kHz, and also simultaneously with a Teledyne LeCroy HDO6104 oscilloscope at a sampling rate of 1 GHz.

3. Results

3.1. *Subsonic (M = 0.3 - 0.8) Free-Stream Turbulence Characterization*

Characterization of the free-stream fluctuations in terms of the spectral content is of importance in wind tunnel measurements. In comparison exercises between experimental data and numerical simulations in a variety of flow configurations, a good understanding of the free-stream noise behavior often helps in supplying physically realistic boundary conditions to the numerical simulations, thereby increasing their fidelity. As discussed above, thermal anemometry techniques are best suited for such measurements, and here we attempt to quantify the free-stream turbulence in the TWM at three different Mach numbers – M = 0.3, 0.5, 0.8 – in the subsonic regime.

The heat transfer from the sensors during operation, which is quantified by the time-resolved anemometer output voltage (V), is in general a function of the mass flow rate ρu (ρ and u are the density and streamwise velocity respectively) and the total temperature T_0. However for the purposes of this analysis we assume any fluctuations in the free-stream total temperature to be negligible in comparison to mass flow fluctuations; the output voltage V is taken to be a non-linear function of ρu alone. At each Mach number, the transfer function was obtained through a calibration exercise where free-stream measurements were made at the set Mach number but over a few different stagnation pressures. Note that the mean mass flow rate increases with stagnation pressure at all

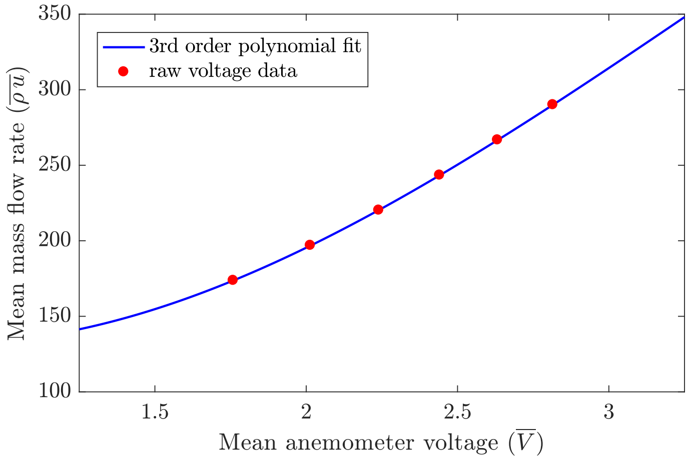

FIGURE 5. A sample calibration curve obtained at M = 0.3 free-stream conditions. The mean mass flow rate as a function of the mean anemometer voltage is fitted to a third-order polynomial to obtain a non-linear transfer function between instantaneous voltage and mass flow rate for the time-resolved data.

Mach numbers. Third-order polynomial functions were found to fit the mean mass flow rate and voltage data sufficiently well. A sample calibration curve at $M = 0.3$ is shown in figure 5 for reference. Thus a transfer function was obtained to translate time-resolved anemometer voltage to mass flow rate fluctuations.

Power spectral density (Φ) of ρu fluctuations in the free-stream estimated using the above outlined procedure at the three different Mach numbers are shown in figure 6. The values for turbulence intensity $I = \sqrt{\overline{(\rho u)'^2}}/\overline{\rho u}$ are also given in the plots for each stagnation pressure condition. Note that here the instantaneous mass flow rate ρu is decomposed into mean and fluctuating components, written as $\overline{\rho u} + (\rho u)'$ respectively. For M = 0.3 and 0.5, a clear increasing trend in the energetic levels of mass flow fluctuations is seen with increase in the stagnation pressure. Given that the local Reynolds number increases with mass flow rate, the observed trend is to be perhaps expected. However, an interesting reversal of this trend is noticed at M = 0.8 – the energetic levels of mass flow rate fluctuations drop with stagnation pressure. Since the total temperature fluctuations were neglected in this analysis, further scrutiny of these results with additional data is required to make firm conclusions at this Mach number.

3.2. *Preliminary Boundary Layer Measurements at* $M = 0.8$

Following free-stream calibration, preliminary boundary layer measurements at $M = 0.8$ were made on the flat plate model. Figure 7 shows the mean and variance (I^2) profiles of the mass flow rate as a function of the wall-normal distance z. The notation $(\cdot)_\infty$ in the figure denote quantities measured in the free-stream. As expected, the mean mass flow rate goes towards zero and the turbulence intensifies moving from the free-stream towards the wall. In the near-wall region, these measurements were limited by sting vibration issues and thereby the peak in turbulence intensity close to the wall was inaccessible. These preliminary results however are a good demonstration of the sensor capabilities, and show the promise of providing well-resolved boundary layer data with improvements in the experimental setup.

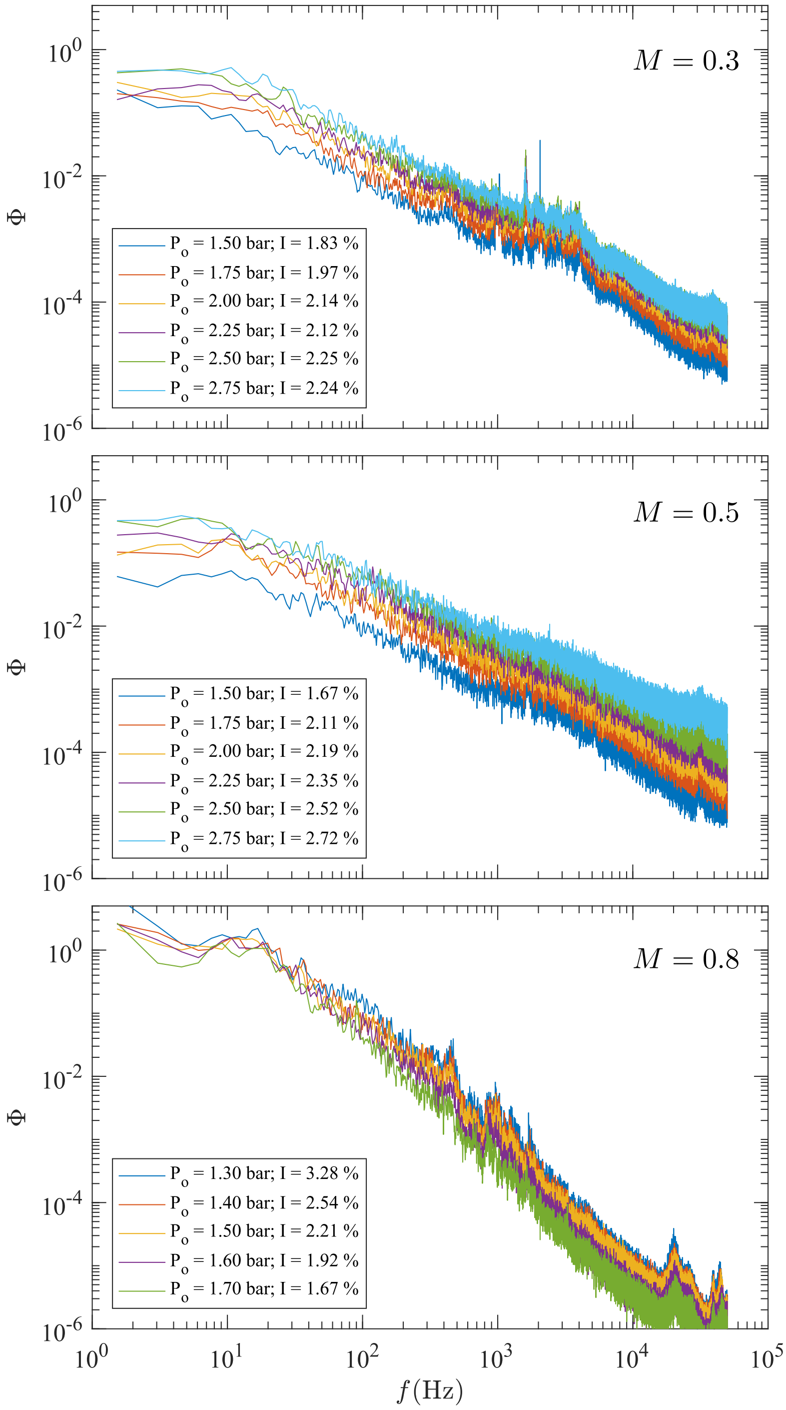

FIGURE 6. Power spectral density (Φ) of free-stream turbulence in the TWM at subsonic Mach numbers. M = 0.3 in top panel, M = 0.5 in center panel, and M = 0.8 in bottom panel.

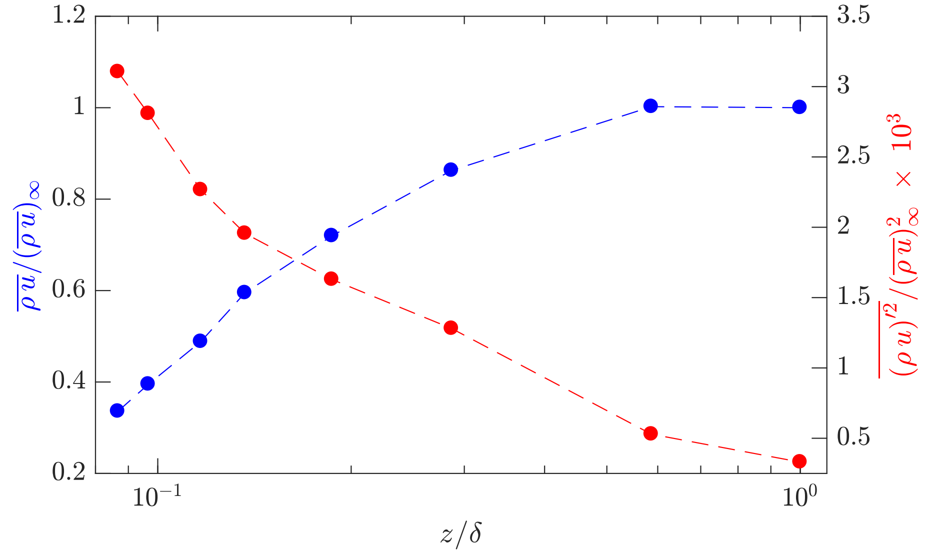

FIGURE 7. Preliminary measurements in a $M = 0.8$ turbulent boundary layer.

3.3. *Simultaneous Mass Flow and Wall-Pressure Correlations at* $M = 0.8$

The interaction between the near-wall and far fields of the boundary layer has been widely studied and has important implications for understanding the complete scaling of the flow. To compare fluctuations in the boundary layer and at the surface, the sensor was placed directly above one of the wall pressure ports at a wall-normal distance of approximately 10% of the boundary layer thickness. The pressure ports, indicated in figure 2, are equipped with Kulite transducers with a frequency response of 25 kHz. The pressure and anemometer voltage signals were then simultaneously recorded and correlated during post-processing.

Due to the different wall-normal locations of the sensor and pressure ports, a time delay in the signals is to be expected based on the streamwise inclination of coherent structures, *i.e.* horseshoe or roll-up vortices. As the frequency response of the nano-scale sensor is higher than the Kulites, the temporal signal was shifted in small increments of t' and correlated with the wall pressure signal using below equation,

$$R(x,y,t') = \frac{\sum_{i=1}^{N} [p_w(x,y) - \overline{p_w}(x,y)][V_i(x,t_i - t') - \overline{V}(x,t_i - t')]}{\sqrt{\sum_{i=1}^{N} [p_w(x,y) - \overline{p_w}(x,y)]^2 \sum_{i=1}^{N} [V_i(x,t_i - t') - \overline{V}(x,t_i - t')]^2}}, \tag{3.1}$$

where p_w represents the wall pressure and i represents the sample index. Note that p_w is directly correlated here with the anemometer voltage V.

Figure 8 shows the correlation coefficient R as a function of the time shift. The sensor is located directly above port 1. Port 2 is located at the same spanwise location as port 1 but at a position 59 mm upstream. The time shift correlation is also calculated for two pressure ports, labeled 3 and 4, that are located symmetrically (55 mm) in the spanwise direction about port 1 (see T-shaped dynamic sensor layout in figure 2). As

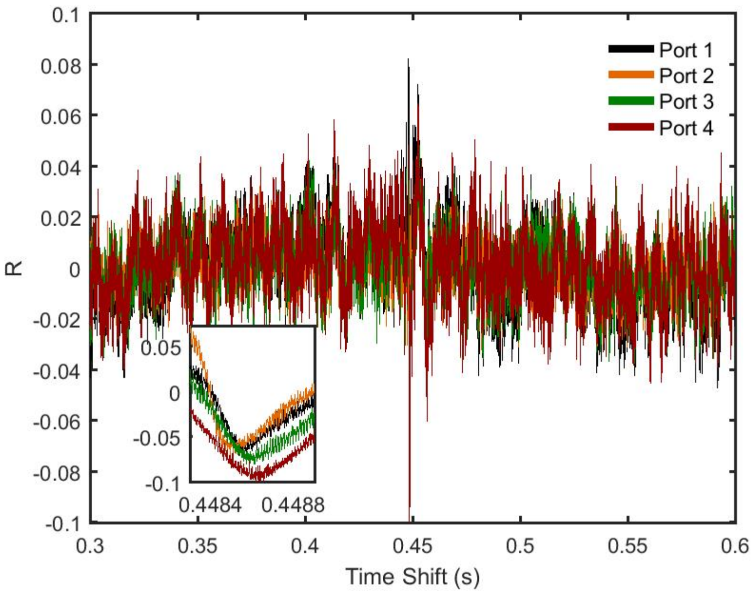

FIGURE 8. Wall pressure and nano-scale sensor signal correlations as a function of time offset t'. The sensor is directly located above port 1, port 2 is 59 mm upstream of port 1. Ports 3 and 4 are symmetrically (55 mm) located in the spanwise direction around port 1. The x-axis refers to time shift of the sensor signal with respect to the wall pressure signal. Inset plot displays a zoomed-in view of correlation peaks.

seen from the figure, the sensor data must be shifted by approximately 0.45 seconds for maximum degree of correlation with the surface pressure fluctuations. This indicates that the correlating turbulent structures leave a footprint at the wall a short time period after they are detected in the far field region by the sensor. Therefore, if the footprint signal is detected further upstream at port 2, then the time shift of the far field signal should be less, which is reflected in the slightly lower time shift seen for port 2 (see zoomed in view in figure 8). Furthermore, the sensor signal also correlates with the spanwise space pressure ports 3 and 4; the correlation peaks for ports 3 and 4 are similarly located.

As both p_w and V are obtained from point measurements, they do not give spatial information about the entire velocity field. Therefore, these two measurements techniques can be combined with full field PIV measurements, with the idea that the instantaneous velocity fields can be correlated with the signals from the wall pressure transducers and the nano-scale sensors. This would not only allow for the correlation of the temporally corresponding wall pressure signals to its velocity vector field, but also makes it possible to correlate a prior or future Kulite pressure data set to that vector field. This makes it possible to track coherent structures up to the temporal resolution of the pressure sensors, while retaining the high quality imaging characteristics of a sCMOS PIV camera.

3.4. *Supersonic (M = 1.2 to 2) Free-Stream Tests*

The sensors were successfully tested in supersonic conditions up to a Mach number of 2 in the TWM. As an example, figure 9 shows the time series data of p_0, M, and V (anemometer signal) from one of the supersonic flow experiments. As previously

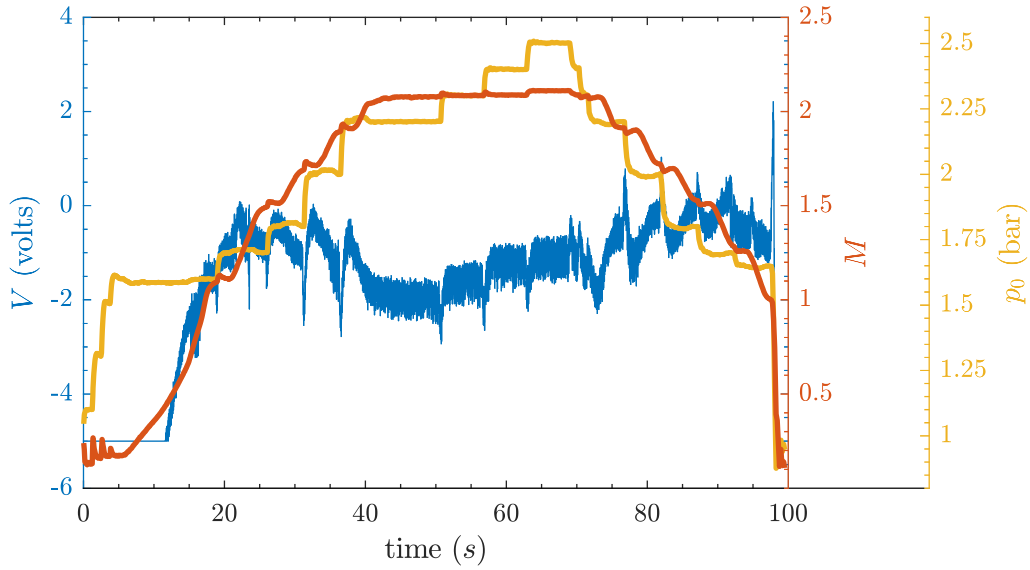

FIGURE 9. Time-resolved data from a supersonic flow experiment.

discussed, supersonic conditions are achieved in the test section starting at a Mach number close to 1 at a relatively low stagnation pressure p_0; this occurs at around $t \approx 20$ s in figure 9. From this point on, p_0 is gradually increased while the nozzle throat area is further decreased to reach $M = 2$ at $t \approx 40$ s. p_0 is further increased in steps at M = 2 to obtain different mass flow rates at fixed Mach number, and corresponding increases in the anemometer output voltage are also clearly seen. Similar to the subsonic cases, this data helps in calibrating the anemometer voltage to estimate mass flow rates. Further, these tests were also repeated at a few different sensor overheat ratios (data not shown here). Varying the overheat ratio allows for the isolation of total temperature fluctuations, which are significant in supersonic conditions, from mass flow fluctuations. This analysis will be the subject of future work.

4. Conclusions

In this report we summarized results from an experimental campaign where novel nano-scale thermal anemometry sensors were tested for the first time in compressible flow conditions, going up to a Mach number of 2. Several new ideas were derived from this experience in terms of further sensor development and better integration techniques into the test facility. The preliminary results show a clear promise towards the developments of robust high-resolution point-measurement capabilities that neatly complement existing particle image velocimetry (PIV) techniques in compressible flows. Research progress along this line would greatly aid in advancing our understanding of compressible shear turbulence at a fundamental level and also contribute towards development of high-fidelity models for numerical studies aimed at various aerodynamic design applications.

Acknowledgments

The authors gratefully acknowledge the catalytic role played by the Sonderforschungsbereich Transregio 40 program in bringing about this collaboration between research groups at Princeton and Bundeswehr Universities. Financial support was provided to SD and KK by the German Research Foundation (DeutscheForschungsgemeinschaft – DFG) under the framework of the Sonderforschungsbereich Transregio 40 to partake in these experiments during the 2017 summer program. We also thankfully acknowledge the organizational support provided by Dr. Christian Stemmer (TU München) as part of the summer program.

References

[1] SMITS, A.J. AND DUSSAUGE, J.P. (2006). *Turbulent shear layers in supersonic flow*. Springer Science & Business Media.

[2] ADRIAN, R.J. (2005). Twenty years of particle image velocimetry. *Experiments in Fluids*, **39**(2), 159–169.

[3] SCARANO, F. (2008). *Overview of PIV in supersonic flows*. Springer Berlin Heidelberg, Berlin, Heidelberg, 445–463.

[4] BAILEY, S.C.C., KUNKEL, G.J., HULTMARK, M., VALLIKIVI, M., HILL, J.P., MEYER, K.A., TSAY, C., ARNOLD, C.B. AND SMITS, A.J. (2010). Turbulence measurements using a nanoscale thermal anemometry probe. *Journal of Fluid Mechanics*, **663**, 160–179.

[5] VALLIKIVI, M., HULTMARK, M., BAILEY, S.C.C. AND SMITS, A.J. (2011). Turbulence measurements in pipe flow using a nano-scale thermal anemometry probe. *Experiments in fluids*, **51**(6), 1521–1527.

[6] FAN, Y., ARWATZ, G., VAN BUREN, T., HOFFMAN, D. AND HULTMARK, M. (2015). Nanoscale sensing devices for turbulence measurements. *Experiments in Fluids*, **56**(7), 138.

[7] HULTMARK, M., VALLIKIVI, M., BAILEY, S. AND SMITS, A. (2012). Turbulent pipe flow at extreme reynolds numbers. *Physical Review Letters*, **108**(9), 094501.

[8] SCHARNOWSKI, S., BOLGAR, I. AND KÄHLER, C.J. (2017). Characterization of turbulent structures in a transonic backward-facing step flow. *Flow, Turbulence and Combustion*, **98**(4), 947–967.

[9] KUNKEL, G., ARNOLD, C. AND SMITS, A. (2006). Development of NSTAP: nanoscale thermal anemometry probe. In: *Proceedings of the 36th AIAA fluid dynamics conference*.

[10] VALLIKIVI, M. AND SMITS, A.J. (2014). Fabrication and characterization of a novel nanoscale thermal anemometry probe. *Journal of Microelectromechanical Systems*, **23**(4), 899–907.